



Contents lists available at ScienceDirect

## Bioorganic &amp; Medicinal Chemistry Letters

journal homepage: [www.elsevier.com/locate/bmcl](http://www.elsevier.com/locate/bmcl)

## Discovery of N-substituted pyridinones as potent and selective inhibitors of p38 kinase

Shaun R. Selness<sup>a,\*</sup>, Rajesh V. Devraj<sup>a</sup>, Joseph B. Monahan<sup>b</sup>, Terri L. Boehm<sup>a</sup>, John K. Walker<sup>a</sup>, Balekudru Devadas<sup>a</sup>, Richard C. Durley<sup>a</sup>, Ravi Kurumbail<sup>c</sup>, Huey Shieh<sup>c</sup>, Li Xing<sup>c</sup>, Michael Hepperle<sup>a</sup>, Paul V. Rucker<sup>a</sup>, Kevin D. Jerome<sup>a</sup>, Alan G. Benson<sup>a</sup>, Laura D. Marrufo<sup>a</sup>, Heather M. Madsen<sup>a</sup>, Jeff Hitchcock<sup>a</sup>, Tom J. Owen<sup>a</sup>, Lance Christie<sup>a</sup>, Michele A. Promo<sup>a</sup>, Brian S. Hickory<sup>a</sup>, Edgardo Alvira<sup>a</sup>, Win Naing<sup>a</sup>, Radhika Bleviss-Bal<sup>a</sup>

<sup>a</sup> Department of Medicinal Chemistry, Pfizer Corporation, 700 Chesterfield Parkway West, Chesterfield, MO 63017, USA

<sup>b</sup> Inflammation Biology, Pfizer Corporation, 700 Chesterfield Parkway West, Chesterfield, MO 63017, USA

<sup>c</sup> Structural and Computational Chemistry, Pfizer Corporation, 700 Chesterfield Parkway West, Chesterfield, MO 63017, USA

## ARTICLE INFO

## Article history:

Received 8 June 2009

Revised 21 August 2009

Accepted 24 August 2009

Available online 27 August 2009

## Keywords:

p38 kinase

Pyridinones

## ABSTRACT

The identification and evolution of a series of potent and selective p38 inhibitors is described. p38 inhibitors based on a *N*-benzyl pyridinone high-throughput screening hit were prepared and their SAR explored. Their design was guided by ligand bound co-crystals of p38 $\alpha$ . These efforts resulted in the identification of **12r** and **19** as orally active inhibitors of p38 with significant efficacy in both acute and chronic models of inflammation.

© 2009 Elsevier Ltd. All rights reserved.

The overexpression of the pro-inflammatory cytokines TNF- $\alpha$  and IL-1 $\beta$  has been linked to the development and progression of several inflammatory diseases such as rheumatoid arthritis (RA) and Crohn's disease.<sup>1</sup> The efficacy demonstrated by several marketed protein therapeutics such as etanercept, adalimumab and infliximab in RA suggests that small molecule modulators of pathways leading to the production of these cytokines could have potential therapeutic benefit.<sup>2</sup> p38 has been identified as a central kinase in the stress induced MAPKAP pathways leading to the production of these key mediators.<sup>3,4</sup> Inhibition of p38 has been shown to reduce the production of cytokines such as TNF- $\alpha$ , IL-6 and IL-8 in monocytic cell systems.<sup>5</sup> In vivo anti-inflammatory activity has been demonstrated with numerous p38 inhibitors in several rodent models of inflammation. This data has driven much research in this area and diverse classes of small molecule inhibitors of p38 have been identified.<sup>6</sup>

We herein describe the identification and generation of highly selective p38 inhibitors from the *N*-benzyl pyridinone high-throughput screening hit, SC-25028, **1**. Recently described inhibitors of p38 kinase such as VX-745, **2**, have demonstrated superior kinase selectivity as compared to historical diaryl heterocyclic inhibitors such as SB-203580, **3** (Fig. 1).<sup>7,8</sup> The enzyme activity of

**1** against p38 $\alpha$  was modest (1  $\mu$ M). However, evaluation of **1** against a panel of 48 kinases revealed that the compound was selective for p38 (less than 30% inhibition at 10  $\mu$ M against the entire panel).

The co-crystal structure of **1** bound to p38 $\alpha$  highlighted the key structural features associated with its binding mode (Fig. 2).<sup>9</sup> A dual hydrogen bond to Met 109 and Gly 110 was observed for **1** which requires a backbone flip of Gly 110. This binding mode is consistent with the induced flip observed with **2** (Fig. 3).<sup>10</sup> The benzyloxy group occupied the lipophilic pocket and the *N*-benzyl group was directed toward the solvent front. This binding mode suggested several structure-based design strategies. These strategies included targeting residues Asp112 and Asn115 with appropriate functionality via substitution on the *N*-benzyl group of **1**. The role of the C3 bromine was probed with simple halogen isosteres.

Metabolic stability of **1** was recognized as a primary liability as revealed by its incubation with human liver microsomes (52% parent remaining after 45 min of incubation). Efforts to improve on the metabolic stability of **1** focused on halogen substitution on the benzyloxy ring and placement of electron-withdrawing groups on the *N*-benzyl ring to block oxidative cleavage of the C–O and C–N bonds.

The general preparation of these *N*-substituted pyridinones is shown in Schemes 1 and 2. Displacement of 4-chloropyridine-1-

\* Corresponding author. Tel.: +1 636 247 6856.

E-mail address: [shaun.r.selness@pfizer.com](mailto:shaun.r.selness@pfizer.com) (S.R. Selness).

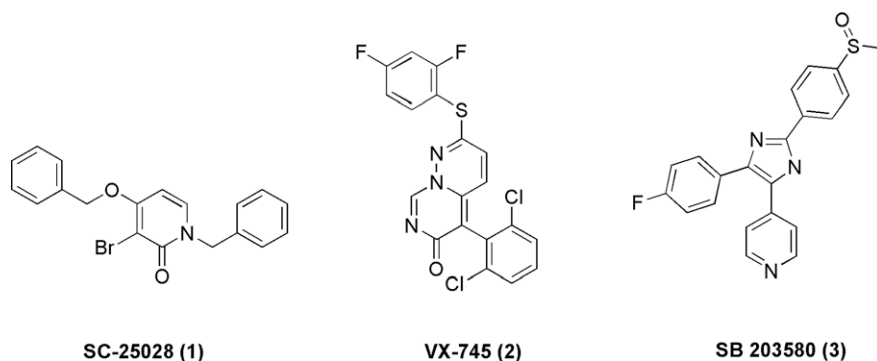
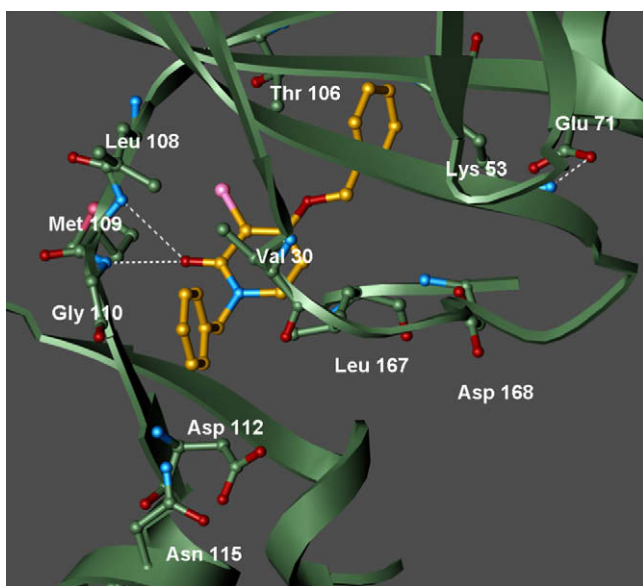
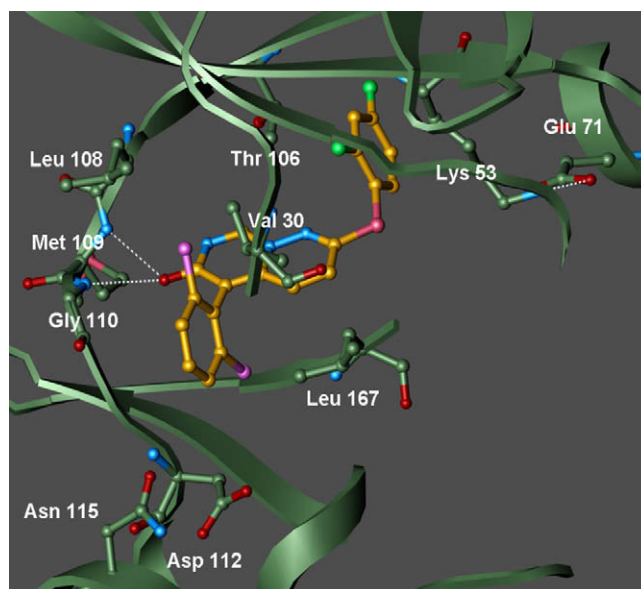


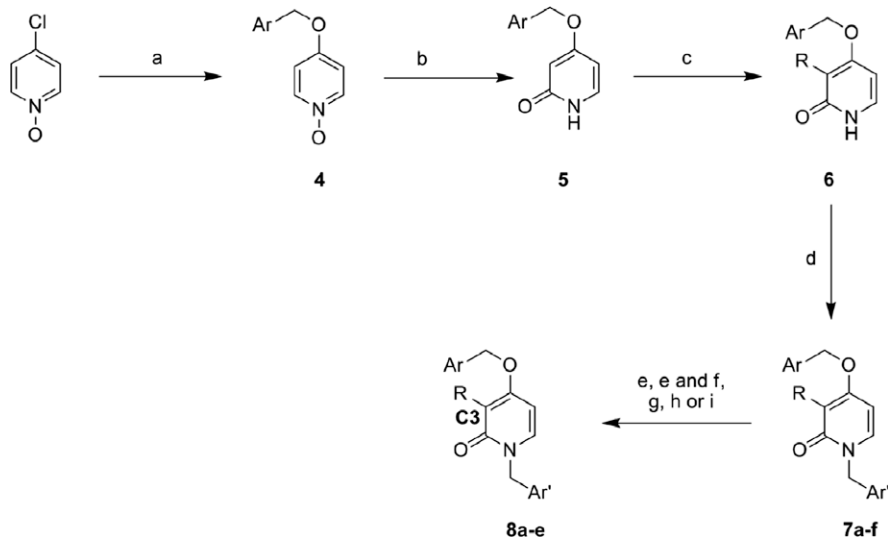
Figure 1. SC-25028, VX-745 and SB-203580.



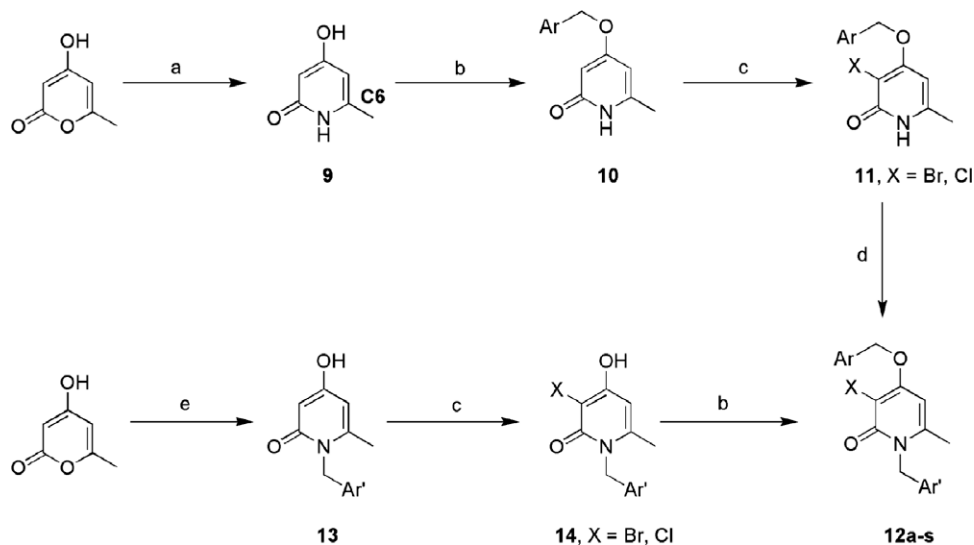
**Figure 2.** Crystal structure of compound **1** bound in the active site of p38α. Crystals of p38α were obtained by soaking experiment. The structure has been refined to a  $R_{\text{free}}$  of 25.1% at 2.15 Å resolution ( $R_{\text{crystal}}$ : 32.1%). Some of the key side chains of p38α are displayed (C: green, N: dark blue and O: red). The inhibitor is represented with carbon, nitrogen, oxygen and bromine atoms displayed in gold, blue, red, and pink, respectively. The hydrogen bonds formed by the inhibitor are shown in dotted white lines.



**Figure 3.** Crystal structure of compound **2** bound in the active site of p38α. Crystals of p38α were obtained by soaking experiment. The structure has been refined to a  $R_{\text{free}}$  of 22.3% at 2.3 Å resolution ( $R_{\text{crystal}}$ : 30.4%). Some of the key side chains of p38α are displayed (C: green, N: dark blue and O: red). The inhibitor is represented with carbon, nitrogen, oxygen, sulfur, fluorine, chlorine and bromine atoms displayed in gold, blue, red, rose, green, purple and pink, respectively. The hydrogen bonds formed by the inhibitor are shown in dotted white lines.



**Scheme 1.** Synthesis of N-benzyl pyridinones from 4-chloropyridine-1-oxide. Reagents and conditions: (a) benzyl alcohol, NaH/DMF, 100 °C; (b) Ac<sub>2</sub>O, reflux then MeOH/H<sub>2</sub>O; (c) Br<sub>2</sub>, AcOH, 0 °C or NBX, AcCN; (d) arylCH<sub>2</sub>X, K<sub>2</sub>CO<sub>3</sub>/DMF 110 °C; (e) vinylSnBu<sub>3</sub>, PdCl<sub>2</sub>(PPh<sub>3</sub>)<sub>2</sub>, DMF, 80 °C; (f) H<sub>2</sub>, Pd/C, EtOH, 1 atm; (g) Me<sub>4</sub>Sn, PdCl<sub>2</sub>(PPh<sub>3</sub>)<sub>2</sub>, DMF; (h) CuI, NaO(CO)CF<sub>3</sub>; (i) Zn(CN)<sub>2</sub>, Pd(OTf)<sub>2</sub>, Zn, racemic-2-di-*t*-butylphosphino-1,1'-binaphthyl, DMAC, 95 °C, 3 h.



**Scheme 2.** Synthesis of *N*-benzyl pyridinones from 4-hydroxy-6-methylpyran-2-one. Reagents and conditions: (a)  $\text{NH}_4\text{OH}$  (aq); (b)  $\text{ArylCH}_2\text{X}$ ,  $\text{K}_2\text{CO}_3/\text{DMF}$ ; (c)  $\text{Br}_2$ ,  $\text{AcOH}$ ,  $0^\circ\text{C}$  or  $\text{NBX}$ ,  $\text{AcCN}$ ; (d)  $\text{ArylCH}_2\text{X}$  or heteroaryl(methylene) halide,  $\text{NaH}/\text{THF}$ , reflux; (e)  $\text{ArylCH}_2\text{NH}_2$  or heteroaryl $\text{CH}_2\text{NH}_2$ ,  $\text{H}_2\text{O}$ , reflux.

oxide with the appropriate benzyl alcohol affords the corresponding aryloxy pyridine-*N*-oxide, **4**. Acetic anhydride mediated rearrangement of **4** produces the pyridinone, **5**. Halogenation of **5** can be accomplished with molecular bromine or  $\text{NBX}$  ( $\text{X} = \text{Br}$ ,  $\text{I}$  or  $\text{Cl}$ ) to yield the corresponding 3-halopyridinone, **6**. Alkylation of **6** with various benzyl halides gives the 3-halo-*N*-substituted pyridinone, **7**. The iodo precursor, **7b**, is converted to the C3 vinyl pyridinone via a Stille coupling reaction to afford pyridinone **8a**. Catalytic hydrogenation of **8a** afforded the C3 ethyl analog, **8b**. The C3 methyl, trifluoromethyl and cyano analogs (**8c–e**) were prepared via metal mediated coupling reactions (Scheme 1).

Two alternative syntheses were pursued to generate a series of 6-methyl-*N*-substituted pyridinone derivatives as outlined in Scheme 2. Condensation of 4-hydroxy-6-methylpyran-1-one with aqueous  $\text{NH}_4\text{OH}$  gives the hydroxy pyridinone, **9**. Alkylation of **9** with a benzyl halide affords the benzyloxy pyridinone, **10**. Halogenation of **10** under the conditions in Scheme 1 generates the 3-halopyridinone, **11**. Initial attempts at alkylation of **11** with a benzyl or heteroaryl(methylene) halide under several conditions resulted in mixtures of *O*- and *N*-alkylated products. We found that the use of  $\text{NaH}/\text{THF}$  favored the formation of the desired *N*-substituted pyridinone, **12**. Alternatively, condensation of 4-hydroxy-6-methylpyran-1-one with a substituted benzyl or heteroaryl(methylene) amine yields the *N*-substituted pyridinone, **13** in moderate to good yields. This condensation was reported to proceed in *n*-butyl alcohol.<sup>11</sup> We observed bis-addition of the amine under these conditions which was avoided by using water as the solvent. This minimized the bis-adduct formation and facilitated isolation of **13**. Installation of the halide is accomplished via treatment with bromine or  $\text{NCX}$  to afford the 3-halo-*N*-substituted pyridinone, **14**. Benzylation of **14** with a substituted benzyl halide provided the desired pyridinone, **12a–f**.

Initially, we investigated the role of the C3 position and its contribution to the activity of the series. Chloro and bromo groups were identified as preferred as shown by the activity of **1** and **7a** (Table 1). The halogen group at C3 occupies a shallow lipophilic pocket adjacent to the deep selectivity pocket as defined by Thr106. Additionally, we used activity against JNK2 to evaluate the potential for kinase selectivity. As shown in Table 1 this series was highly selective versus JNK2. Based on historical data from both the diaryl five-membered heterocycles such as **3** and the new class of fused ring systems such as **2**, a limited number of halo

substituted benzyloxy groups were investigated.<sup>7,8</sup> We concluded that the 2,4-difluorobenzyloxy group was optimal for potency and focused our attention on the *N*-benzyl substituent.

As shown in Table 2, *ortho*-substituted *N*-benzyl groups were not tolerated compared to the *meta*- or *para*-substituted *N*-benzyl groups (**12a–f**). Carboxamide substitution in the *para*-position afforded several potent compounds (**12f**, **12h–k**) with activity below 100 nM. Compounds **12h**, **12i** and **12k** were shown to be active in a rat lipopolysaccharide (rLPS) model of inflammation.<sup>12,13</sup> A series of heterocyclic replacements were investigated in an effort to reduce the log *D* of the series and to improve the metabolic stability of the series. The pyridines **12o** and **12p** showed modest activity against p38 but exhibited good activity in rLPS. This was attributed to improved metabolic stability and better bioavailability relative to **1**.

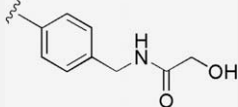
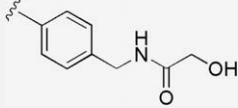
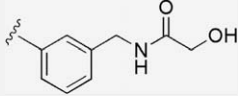
In an effort to engage Asp 112 the amines **16**, **17**, **18** and **19** were prepared (via  $\text{BH}_3/\text{dimethylsulfide}$  reductions of **12b**, **12c**, **12g** and **12h**, respectively). Although their enzyme activities against p38 $\alpha$  did not improve relative to the neutral carboxamides, significant *in vivo* activity in rLPS was achieved for **16** and **19**. Investigation of neutral analogs of **16** and **17** identified **20**, **21** and **22** as potent inhibitors of p38 $\alpha$ . These were prepared via acylation of **16**, **17** and the chloro analog of **17** with glycolic acid.

**Table 1**  
Potency and selectivity (as measured by inhibition of JNK2) of 4-benzyloxy-3-halo-*N*-substituted pyridinones and 4-benzyloxy-3-alkyl-*N*-substituted pyridinones

Compd	R	Ar	Ar'	p38 $\alpha$ IC <sub>50</sub> ( $\mu\text{M}$ )	JNK2 IC <sub>50</sub> ( $\mu\text{M}$ )
<b>1</b>	Br	Ph	Ph	0.68	>200
<b>2</b>				0.07	>200
<b>3</b>				0.07	0.32
<b>7a</b>	Cl	Ph	Ph	0.90	NA
<b>7b</b>	I	Ph	Ph	3.10	>200
<b>7c</b>	H	Ph	Ph	43	>200
<b>7d</b>	Br	4-Cl-Ph	4-F-Ph	1.90	>200
<b>7e</b>	Br	4-F-Ph	3-F-Ph	0.62	>200
<b>7f</b>	Br	2,4-DiF-Ph	3-F-Ph	0.13	>200
<b>8a</b>	$\text{CHCH}_2$	Ph	Ph	72	>200
<b>8b</b>	Et	Ph	Ph	6.1	>200
<b>8c</b>	Me	Ph	Ph	5.3	>200
<b>8d</b>	$\text{CF}_3$	Ph	3-F-Ph	50	>200
<b>8e</b>	CN	2,4-DiF-Ph	3-F-Ph	9.9	>200

NA—not assessed.

**Table 2**  
Potency and in vivo activity (as measured by inhibition of TNF $\alpha$  in rLPS) of 4-(halo-benzyloxy)-3-halo-N-substituted benzyl pyridinones and substituted 4-(halo-benzyloxy)-3-halo-N-substituted heteroaryl-methylene pyridinones<sup>13</sup>

Compd	X	Ar	Ar'	p38 $\alpha$ IC <sub>50</sub> ( $\mu$ M)	JNK2 IC <sub>50</sub> ( $\mu$ M)	hPBM IC <sub>50</sub> ( $\mu$ M)	% rLPS TNF $\alpha$ Inhibition @-4 h @ (mpk)
12a	Br	2,4-DiF-Ph	2-CN-Ph	1.20	>200	NA	NA
12b	Br	2,4-DiF-Ph	3-CN-Ph	0.11	>200	NA	NA
12c	Br	2,4-DiF-Ph	4-CN-Ph	0.19	>200	0.118	NA
12d	Br	2,4-DiF-Ph	2-NH <sub>2</sub> C(=O)-Ph	2.67	>200	NA	NA
12e	Br	2,4-DiF-Ph	3-NH <sub>2</sub> C(=O)-Ph	0.27	167	NA	NA
12f	Br	2,4-DiF-Ph	4-NH <sub>2</sub> C(=O)-Ph	0.022	>200	0.046	40 (5)
12g	Br	2,4-DiF-Ph	3-NMe <sub>2</sub> C(=O)-Ph	0.25	>200	NA	0 (5)
12h	Br	2,4-DiF-Ph	4-NMe <sub>2</sub> C(=O)-Ph	0.066	>200	0.044	69 (5)
12i	Cl	2,4-DiF-Ph	4-NMe <sub>2</sub> C(=O)-Ph	0.079	>200	NA	79 (5)
12j	Br	2,4-DiF-Ph	3-NMeHC(=O)-Ph	0.20	>200	0.115	0 (5)
12k	Br	2,4-DiF-Ph	4-NMeHC(=O)-Ph	0.025	>200	0.13	84 (5)
12l	Br	4-F-Ph	2-Pyridine	1.00	>200	NA	0 (20)
12m	Br	4-F-Ph	3-Pyridine	0.38	>200	NA	30 (20)
12n	Br	4-F-Ph	4-Pyridine	0.39	>200	NA	0 (20)
12o	Br	2,4-DiF-Ph	3-Pyridine	0.15	>200	NA	81 (20)
12p	Br	2,4-DiF-Ph	4-Pyridine	0.21	>200	NA	80 (20)
12q	Br	2,4-DiF-Ph	2-(5-Me-pyrazine)	0.45	>200	0.576	80 (20)
12r	Br	2,4-DiF-Ph	2-(5-HOCH <sub>2</sub> -pyrazine)	0.45	>200	0.566	89 (30)
12s	Br	2,4-DiF-Ph	5-(2-Me-pyrimidine)	0.18	>200	NA	63 (5)
15	Br	2,4-DiF-Ph	2-H <sub>2</sub> NCH <sub>2</sub> -Ph	1.26	>200	NA	NA
16	Br	2,4-DiF-Ph	3-H <sub>2</sub> NCH <sub>2</sub> -Ph	0.065	>200	NA	90 (20)
17	Br	2,4-DiF-Ph	4-H <sub>2</sub> NCH <sub>2</sub> -Ph	0.12	>200	0.039	57 (5)
18	Br	2,4-DiF-Ph	3-Me <sub>2</sub> NCH <sub>2</sub> -Ph	0.063	>200	0.101	61 (5)
19	Br	2,4-DiF-Ph	4-Me <sub>2</sub> NCH <sub>2</sub> -Ph	0.059	>171	0.044	87 (5)
20	Br	2,4-DiF-Ph		0.046	>200	0.023	93 (5)
21	Cl	2,4-DiF-Ph		0.055	>200	0.028	69 (5)
22	Br	2,4-DiF-Ph		0.049	>200	0.102	32 (15)

NA—not assessed.

Compound **20** possessed significant in vivo activity in rLPS. Assessment of the metabolic stability (as measured by incubation with human and rat microsomes) of a series of pyridinones indicated that significant improvements were achieved for several analogs when compared to **1** (Table 3). The relatively low stabilities observed for compounds **12h** and **18** are attributed to demethylation of each to their more stable metabolites, **12f** and **16**, respectively. Both **12r** and **19** were profiled against a panel of over 200 kinases to assess their selectivities. The compounds showed no significant

cross-reactivity with any of the kinases tested with the exception of p38 $\beta$  (5–10 more selective for p38 $\alpha$  vs p38  $\beta$ ; Table 4).

Several pyridinones were selected for assessment of their pharmacokinetic profiles in male Sprague–Dawley rats (Table 5).<sup>13</sup> A range of clearances were observed for the compounds from low to high. Characterization of plasma samples after oral dosing of **12q** indicated that the major metabolite is the longer-lived **12r**. Similarly, analysis of plasma samples after oral dosing of **19** revealed that the mono-methylamine, **23**, and primary amine, **17** were generated (Fig. 4). Both **17** and **23** demonstrated activity against p38 $\alpha$  (IC<sub>50</sub>s of 120 nM and 52 nM, respectively), activity in hPBMcs (IC<sub>50</sub>s of 59 nM and 49 nM) and were active in rLPS at -4 h at 5 mpk (95% and 91%, respectively). Evaluation of **23** against JNK2 indicated that it was not very potent (IC<sub>50</sub> = 191  $\mu$ M).

Compounds **12r** and **19** were evaluated in a rat Strep Cell Wall (rSCW) model of chronic inflammation (Table 6). Both compounds demonstrated significant efficacy in this model. The higher dose required for **12r** is attributed to its inferior potency against p38 $\alpha$  whereas the activity of **19**, in spite of its high clearance, is attributed to the generation of the active metabolites, **23** and **17**.

In summary, a series of potent, selective and stable inhibitors of p38 $\alpha$  were generated from a high-throughput screening hit that was metabolically unstable and moderately active against p38 $\alpha$ . This new class of inhibitors exhibit a unique binding mode which imparts a high degree of selectivity for p38 $\alpha$  over other kinases. These compounds demonstrated significant activity in both acute

**Table 3**  
Metabolic stability (percent remaining after incubation with human or rat liver microsomes for 45 min) of selected pyridinones<sup>14</sup>

Compd	cLog D	HLM (% remaining)	RLM (% remaining)
1	3.81	52	3
7e	3.92	76	26
7f	4.01	48	16
12f	3.07	89	94
12h	2.76	59	51
12k	3.19	75	63
12q	2.51	98	95
12r	0.86	96	100
16	1.49	89	99
18	2.97	50	39
19	2.91	57	53
20	2.88	73	82

**Table 4**Kinase selectivity panel for **12r** and **19** (percent inhibition <50% at 10  $\mu$ M for all kinases tested, except for p38 $\alpha$  and p38 $\beta$ )

CAMK1	CDK5/p35	FGFR3 K650E	HGK	PDGFR alpha	MSK2
CDK7/cyclin H/MNAT1	CHK1	FGFR4	KHS1	PDGFRA D842V	MSK1
CDK9/cyclin T1	CHK2	FGR	ERK2	PDGFRA T674I	RSK4
IKK alpha	CLK1	FLT1	JNK3	PDGFRA V561D	p70S6K
DAPK1	CLK2	FLT3	p38 beta 82; 99	PDGFR beta	SGK1
GSG2	CLK3	FLT3 D835Y	p38 gamma	PDK1	SGK2
IRAK1	CSF1R	FLT4	p38 delta	PDK1 Direct	SGK3
LRRK2	CSK	mTOR	p38 alpha 100; 100	PHKG1	SNF1LK2
LRRK2 G2019S	CSNK1A1	FRK	p38 alpha Direct 100; 100	PHKG2	SRC
NUAK1	CSNK1D	FYN	ERK1	PIM1	SRC N1
ABL1	CSNK1E	GRK4	JNK1	PIM2	Srm
ABL1 E255K	CSNK1G1	GRK5	JNK2	PRK1	SRPK1
ABL1 G250E	CSNK1G2	GRK6	MAPKAPK2	PLK1	SRPK2
ABL1 T315I	CK1 gamma 3	GRK7	MAPKAPK3	PLK2	TSSK2
ABL1 Y253F	CK2 alpha 1	GSK3A	PRAK	PLK3	TSSK1
ABL2	CK2 alpha 2	GSK3B	MARK1	PKA	MSSK1)
ALK4	ZIPK	HCK	MARK2	PKC alpha	MST3
GRK2	DCK2	HIPK1	MARK3	PKC beta I	YSK1
GRK3	DYRK1A	HIPK2	MARK4	PKC beta II	MST2)
AKT1	DYRK1B	HIPK4	MATK	PKC delta	MST1)
AKT2	DYRK3	IGF1R	MELK	PKC epsilon	SYK
AKT3	DYRK4	IKK beta	MERTK	PKC gamma	TAO1
ALK	EEF2K	IKK epsilon	cMet	PKC eta	TBK1
AMPK A1/B1/G1	EGFR (ErbB1)	INSR	MET M1250T	PKC iota	Tie2
AMPK A2/B1/G1	EGFR (ErbB1) L858R	INSRR	MINK1	PKD3	TYK2
AURKA	EGFR (ErbB1) L861Q	IRAK4	RON	PKC theta	RSE
AURKB	EGFR (ErbB1) T790M	ITK	MST4	PKC zeta	YES1
AURKC	EGFR (ErbB1) T790M	JAK1	MUSK	PKC mu	ZAP70
AXL	EPHA1	JAK2	MYLK2	PKD2	
BLK	EPHA2	JAK2 JH1 JH2	NEK1	PRKG1	
BMX	EPHA3	JAK2 JH1 JH2 V617F	NEK2	PKG2	
BRAF	EPHA4	JAK3	NEK4	PRKX	
BRAF V599E	EPHA5	KDR (VEGFR2)	NEK6	FAK	
BRK1	EPHA8	KIT	NEK7	FAK2	
BTK	EPHB1	KIT T670I	NEK9	Brk	
CAMK1D	EPHB2	LCK	TRKA	cRAF	
CAMK2A	EPHB3	LTK (TYK1)	TRKB	RET	
CAMK2B	EPHB4	LYN A	TRKC	RET V804L	
CAMK2D	ERBB2 (HER2)	LYN B	PAK1	RET Y791F	
CAMK4	ERBB4 (HER4)	MEK1	PAK2	ROCK1	
MRCKA	FER	MEK2	PAK3	ROCK2	
MRCKB	FES (FPS)	MKK6	PAK4	ROS1	
CDK1/cyclin B	FGFR1	COT	PAK6	RSK1	
CDK2/cyclin A	FGFR2	MLK1	PAK7 (KIAA1264)	RSK3	
CDK5/p25	FGFR3	GCK	PASK	RSK2	

**Table 5**Rat pharmacokinetics (male Sprague–Dawley) of selected pyridinones<sup>13</sup>

Compd	CL (ml/min/kg)	$t_{1/2}$ (h)	F (%)
<b>12q</b>	21.50	0.39	30
<b>12r</b>	6.25	4.71	44
<b>19</b>	70	4.97	91
<b>20</b>	26.2	4.1	33

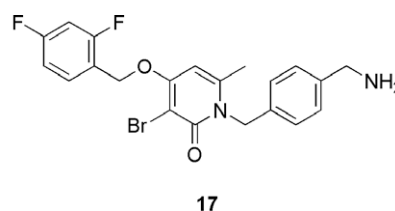
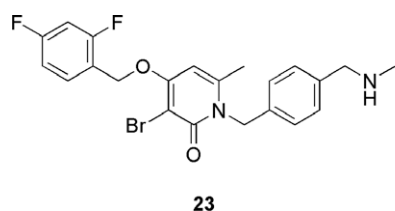
**Table 6**Efficacy in rat Strep Cell Wall (rSCW, female Lewis) of selected pyridinones<sup>11</sup>

Compd	Dose (mpk)	Inhibition of paw swelling (%)
<b>12r</b>	120	87
<b>19</b>	60	88

**Acknowledgements**

We acknowledge the reviewers for providing feedback on the incorporation of key data. We acknowledge Sheri Bonar for generating the hPBMC data. We acknowledge Elizabeth Webb and Gary Anderson for conducting the rLPS and rSCW experiments.

(rLPS) and chronic (rSCW) models of inflammation. Forthcoming publications will describe additional improvements in potency and pharmacokinetic profiles of this pyridinone class of p38 $\alpha$  inhibitors.

**Figure 4.** Observed metabolites of **19**.

## References and notes

1. (a) Arend, W. P.; Dayer, J. M. *Arthritis Rheum.* **1990**, *33*, 305; (b) Firestein, G. S.; Alvaro-Gracia, J. M.; Maki, R. J. *Immunol.* **1990**, *144*, 3347; (c) Rutgeerts, P.; D'Haens, G.; Targan, S.; Vasilias, E.; Hanauer, S. B.; Present, D. H.; Mayer, L.; Van Hogeand, R. A.; Braakman, T.; DeWoody, K. L.; Shaible, T. F.; Van Deventer, S. J. H. *Gastroenterology* **1999**, *117*, 761.
2. Ulfgrén, A. K.; Andersson, U.; Engström, M.; Klareskog, L.; Maini, R. N.; Taylor, P. C. *Arthritis Rheum.* **2000**, *43*, 2391.
3. Foster, M. L.; Halley, F.; Souness, J. E. *Drug News Perspect.* **2000**, *13*, 488.
4. Lee, J. C.; Laydon, J. T.; McDonnell, P. C.; Gallagher, T. F.; Kumar, S.; Green, D.; McNulty, D.; Blumenthal, M. J.; Heys, J. R.; Landvatter, S. W.; Strickler, J. E.; McLaughlin, M. M.; Siemens, I. R.; Fisher, S. M.; Livi, G. P.; White, J. R.; Adams, J. L.; Young, P. R. *Nature* **1994**, *372*, 739.
5. (a) Cohen, P. *Trends Cell Biol.* **1997**, *7*, 353; (b) Widmann, C.; Gibson, S.; Jarpe, M. B.; Johnson, G. L. *Physiol. Rev.* **1999**, *79*, 143; (c) Ono, K.; Han, J. *Cell Signal.* **2000**, *12*, 1; (d) Johnson, G. L.; Lapadat, R. *Science* **2002**, *298*, 1911.
6. (a) Jackson, P. F.; Bullington, J. L. *Curr. Top. Med. Chem.* **2002**, *2*, 1011; (b) Natarajan, S. R.; Doherty, J. B. *Curr. Top. Med. Chem.* **2005**, *5*, 987.
7. Bemis, G. W.; Salituro F. G.; Duffy, J. P.; Cochran, J. E.; Harrington, E. M.; Murcko, M. A.; Wilson, K. P.; Su, M.; Galullo, V. P. US Patent 7365,072 B2, 2008.
8. Adams, J. L.; Boehm, J. C.; Kassis, S.; Gorycki, P. D.; Webb, E. F.; Hall, R.; Sorenson, M.; Lee, J. C.; Ayrton, A.; Griswold, D. E.; Gallagher, T. A. *Bioorg. Med. Chem. Lett.* **1998**, *8*, 3111.
9. The atomic coordinates for the X-ray structure of p38a in complex with **1** have been deposited in the RCSB: rcsb id code—a RCSB053406; PDB code—3HP2.
10. The atomic coordinates for the X-ray structure of p38a in complex with **2** have been deposited in the RCSB: rcsb id code—RCSB053409; PDB code—3HP5.
11. Castillo, S.; Ouadahi, H.; Herault, V. *Bull. Soc. Chim. Fr.* **1982**, 7–8, 257.
12. Compounds were pre-dosed in male Lewis rats at various time points prior to an iv challenge with lipopolysaccharide. Blood was drawn 1.5 h post-challenge and TNF- $\alpha$  levels were evaluated by ELISA.
13. The Pfizer Institutional Animal Care and Use Committee reviewed and approved the animal use in these studies. The animal care and use program is fully accredited by the Association for Assessment and Accreditation of Laboratory Animal Care, International.
14. Metabolic stability was assessed in vitro by incubating 2  $\mu$ M test compound with human or rat liver microsomes, NADPH and buffer at 37 °C for 45 min and measuring percent compound remaining by a precipitation procedure followed by LC/MS analysis.